inorganic compounds

Monoclinic AlPO$_4$ tridymite at 473 and 463 K from X-ray powder data

Heribert A. Graetsch

Institut für Geologie, Mineralogie und Geophysik, Ruhr-Universität Bochum, D-44780 Bochum, Germany
Correspondence e-mail: heribert.graetsch@ruhr-uni-bochum.de

Upon cooling from its hexagonal high-temperature modification, AlPO$_4$ (aluminium phosphate) tridymite successively transforms to several displacively distorted forms, including a normal structure–incommensurate–lock-in phase transition sequence. The space-group symmetries in this series are $P112_1$, $P112_1(\alpha\beta0)$ and $P2_12_12_1$, respectively. The distortion pattern of the intermediate $P112_1$ phase can be described as alternate shifts of adjacent layers of tetrahedra coupled with tilting of the tetrahedra. The symmetry and direction of the shifts are different from the analogous SiO$_2$ tridymite modification. The atomic displacement parameters of the O atoms are strongly anisotropic due to thermal motions of the rigid tetrahedra. Condensation of a lattice vibration mode results in the formation of an incommensurate structural modulation below 473 K. The 3+1 superspace-group symmetry of the modulated phase is $P112_1(\alpha\beta0)$.

Comment

Similar to silica tridymite, isotypic AlPO$_4$ tridymite shows a cascade of several phase transitions at elevated temperatures (Spiegel *et al.*, 1990). For SiO$_2$, the following space-group symmetries and crystal structures of the high-temperature modifications are known: $P6_3/mmc \leftrightarrow C222_1 \leftrightarrow P112_1(\alpha\beta0)$ $\leftrightarrow P2_12_12_1 \leftrightarrow Cc$ and $F1$ (in order of decreasing temperature). Pryde & Dove (1998) ascribed the origin of the phase transitions to the successive condensation of different rigid unit modes. For isoelectronic AlPO$_4$, only the crystal structure of the hexagonal high-temperature modification has been refined so far (Graetsch, 2001b). The symmetry is reduced to $P6_3mc$ with respect to $P6_3/mmc$ for the silica analogue due to the ordered distribution of Al and P over the tetrahedral sites.

X-ray powder diffraction revealed the sequence of displacive transitions as $P6_3mc \leftrightarrow P112_1 \leftrightarrow P112_1(\alpha\beta0) \leftrightarrow P2_12_12_1$ $\leftrightarrow Pc$ and $F1$ for AlPO$_4$ tridymite. The present communication reports the results of Rietveld refinements of the crystal structures of the intermediate $P112_1$ phase (which replaces the $C222_1$ phase of SiO$_2$ tridymite) and the average structure of the incommensurate $P112_1(\alpha\beta0)$ phase in order to work out the structural differences with respect to the silica counterparts.

The crystal structure of hexagonal high-temperature AlPO$_4$ tridymite is made up of alternating corner-sharing AlO$_4$ and PO$_4$ tetrahedra which form six-membered rings of tetrahedra (Fig. 1a). Viewed along the hexagonal c axis, the rings are in eclipsed positions for hexagonal tridymite, whereas in monoclinic high-temperature tridymite ($P112_1$) below 573 K, whole neighboring layers are shifted with respect to each other (Figs. 1b and 1c). The stiff tetrahedra are tilted simultaneously. The hexagonal–monoclinic transition is gradual. Shift and tilting become larger with decreasing temperature.

The situation is similar in the orthorhombic silica analogue ($C222_1$), however, the shift direction is different from that of monoclinic AlPO$_4$ tridymite (Figs. 1b and 1c). The magnitude of the shift is almost the same in both cases: 0.47 Å for SiO$_2$ at 493 K and 0.45 Å for AlPO$_4$ at 473 K. The thermal displacement parameters of the O atoms are strongly anisotropic, whereas those of Al and P at the centers of the tetrahedra are almost spherical (Fig. 2). This indicates that the structure of monoclinic AlPO$_4$ tridymite is dynamically disordered like
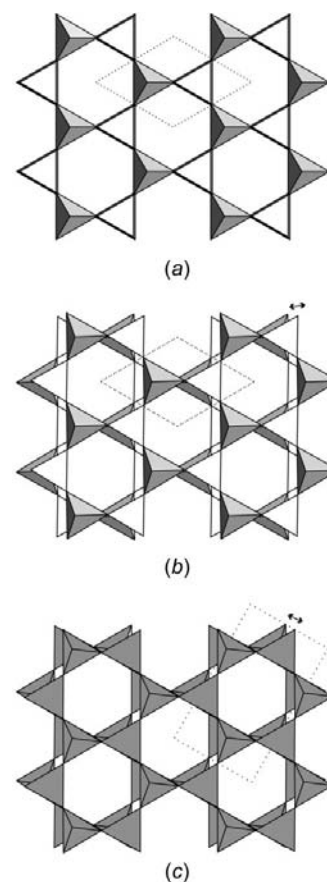

Figure 1
Polyhedral representations of tridymite at various temperatures, viewed along the c axis. (*a*) Hexagonal AlPO$_4$ tridymite at 593 K, (*b*) monoclinic AlPO$_4$ tridymite at 473 K and (*c*) orthorhombic SiO$_2$ tridymite at 573 K (after Kihara *et al.*, 1986). Key: shaded tetrahedra, AlO$_4$; white, PO$_4$; gray, SiO$_4$. The shapes of the unit cells are shown by dotted lines. The small arrows indicate the direction of the shift of the layers of tetrahedra in (*b*) and (*c*).

hexagonal $AlPO_4$ tridymite and that the thermal motions are probably dominated by the rigid-unit modes of the tetrahedra (*cf.* Pryde & Dove, 1998). Elastic diffraction can yield only a time-averaged picture of the structure. As a result, the sizes of the tetrahedra appear to be too small and the inter-tetrahedral $Al-O-P$ angles too large. However, due to reduced thermal vibrations in the monoclinic phase, the latter are no longer straight, as for the average structure of hexagonal $AlPO_4$ tridymite. The $T-O-T$ angle parallel to the *c* axis is larger ($179°$) than those in the perpendicular direction (166, 171 and $161°$).

The appearance of very weak satellite reflections around the main reflections below 473 K (Fig. 3) indicates the formation of an incommensurate modulation. A similar form of silica tridymite exists in the temperature range between about 493 and 423 K. The temperature-dependent modulation consists of wavy tilting and rotations of the tetrahedra (Nukui *et al.*, 1979; Graetsch, 2001*a*).

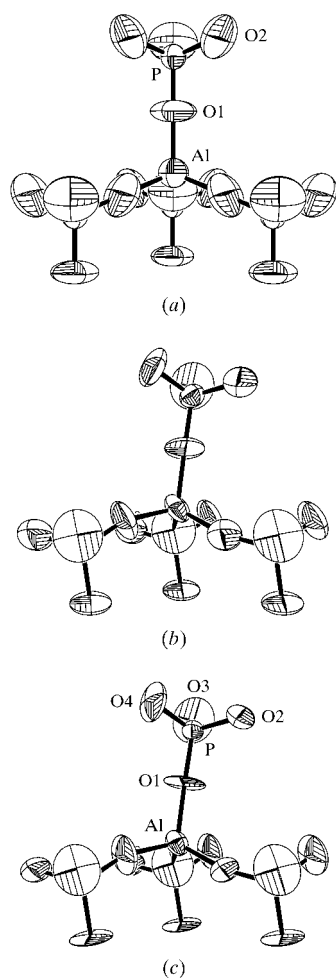The 3+1 superspace group is $P112_1(\alpha\beta0)$ for both the $AlPO_4$ and SiO_2 incommensurate tridymites. The normal–incommensurate transition is gradual in both cases but involves a change of symmetry for the average structure of SiO_2 tridymite [$C222_1 \leftrightarrow P112_1(\alpha\beta0)$] which is not observed for $AlPO_4$ tridymite [$P112_1 \leftrightarrow P112_1(\alpha\beta0)$]. The atomic displacement parameters of the O atoms in the average structure of incommensurate $AlPO_4$ tridymite are highly anisotropic (Fig. 3), similar to the modifications at higher temperatures. However, the average structure represents both static and dynamic contributions. The static component increases as the thermal motions are reduced in the temperature range from 473 to 373 K, leading to an increase in intensity of the satellite reflections.
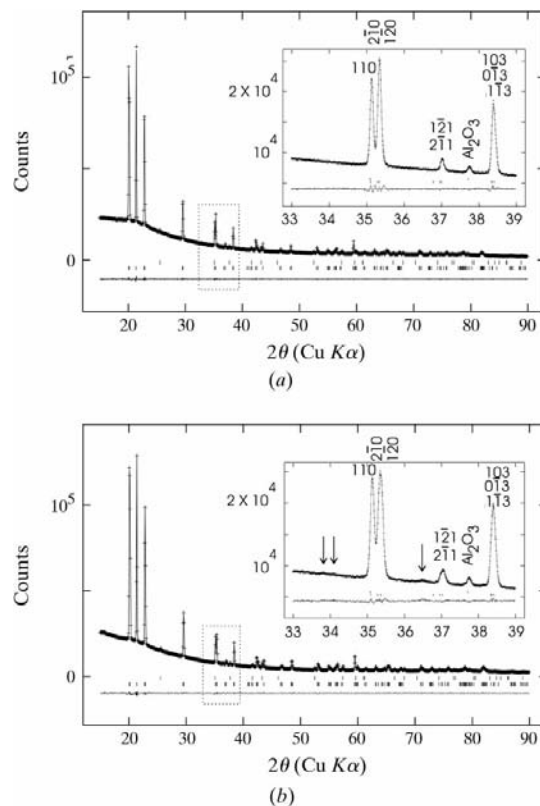

Figure 3
Comparison of the observed (crosses) and calculated (solid line) powder diffraction patterns of high-temperature $AlPO_4$ tridymite (*a*) at 473 K and (*b*) at 463 K. The arrows in (*b*) point to weak satellite reflections. The difference patterns are shown below. The short bars indicate the positions of the reflections of corundum (first row) and tridymite (second row).

Experimental

$AlPO_4$ tridymite was prepared by annealing non-crystalline $AlPO_4$ (Merck No. 1.01098.1000) at 1223 K for 1 d. The sample was transformed to hexagonal high tridymite by heating to 593 K with a hot-air jet directed perpendicular to the capillary and then cooling to the desired temperatures. A gradual phase transition from hexagonal to monoclinic symmetry was observed near 573 K. Below 473 K the appearance of weak satellite reflections indicated the formation of an incommensurate modulation. Two powder data sets were collected at 473 (10) and 463 (10) K in order to refine the crystal structure of the normal phase and the average structure of the incommensurate phase, respectively. The sample contained about 4 wt% corundum, which was refined together with the tridymite phase.

Figure 2
ORTEP-3 (Farrugia, 1997) plots of $AlPO_4$ tridymite viewed normal to (100) and shown with 50% probability displacement ellipsoids. The AlO_4 group is surrounded by four PO_4 groups and is shown as (*a*) the hexagonal phase at 593 K, (*b*) the monoclinic basic structure at 473 K and (*c*) the average structure of the incommensurate phase at 463 K.

AlPO₄ tridymite at 473 K

Crystal data

AlPO₄
$M_r = 121.95$
Monoclinic, $P2_1$
$a = 5.0800 (2)$ Å
$b = 5.0748 (2)$ Å
$c = 8.3009 (3)$ Å
$\gamma = 119.6253 (2)°$
$V = 186.025 (13)$ Å³
$Z = 2$

$D_x = 2.177 (1)$ Mg m⁻³
Cu $K\alpha$ radiation
$\mu = 7.9$ mm⁻¹
$T = 473$ K
White
Specimen shape: cylinder
$40 \times 0.5 \times 0.5$ mm
Specimen prepared at 1223 K
Particle morphology: plate-like

Data collection

Siemens D5000 diffractometer
Specimen mounting: powder filled into a 0.5 mm glass capillary

Specimen mounted in transmission mode
$2\theta_{min} = 15$, $2\theta_{max} = 90°$
Increment in $2\theta = 0.008°$

Refinement

Refinement on I_{net}
$R_p = 0.011$
$R_{wp} = 0.015$
$R_{exp} = 0.011$
$S = 1.36$
$2\theta_{min} = 15$, $2\theta_{max} = 90°$
Increment in $2\theta = 0.008°$
Wavelength of incident radiation: 1.54056 Å

Excluded region(s): none
Profile function: pseudo-Voigt
194 reflections
77 parameters
$w = 1/[y(obs)]^{1/2}$
$(\Delta/\sigma)_{max} = 0.01$
Preferred orientation correction: none

AlPO₄ tridymite at 463 K

Crystal data

AlPO₄
$M_r = 121.95$
Monoclinic, $P2_1$
$a = 5.0803 (2)$ Å
$b = 5.0703 (2)$ Å
$c = 8.2992 (3)$ Å
$\gamma = 119.6037 (3)°$
$V = 185.868 (13)$ Å³
$Z = 2$

$D_x = 2.179$ Mg m⁻³
Cu $K\alpha$ radiation
$\mu = 7.9$ mm⁻¹
$T = 463$ K
White
Specimen shape: cylinder
$40 \times 0.5 \times 0.5$ mm
Specimen prepared at 1223 K
Particle morphology: plate-like

Data collection

Siemens D5000 diffractometer
Specimen mounting: filled into a 0.5 mm glass capillary

Specimen mounted in transmission mode
$2\theta_{min} = 15$, $2\theta_{max} = 90°$
Increment in $2\theta = 0.008°$

Refinement

Refinement on I_{net}
$R_p = 0.011$
$R_{wp} = 0.015$
$R_{exp} = 0.011$
$S = 1.38$
$2\theta_{min} = 15$, $2\theta_{max} = 90°$
Increment in $2\theta = 0.008°$
Wavelength of incident radiation: 1.54056 Å

Excluded region(s): none
Profile function: pseudo-Voigt
194 reflections
77 parameters
$w = 1/[y(obs)]^{1/2}$
$(\Delta/\sigma)_{max} = 0.01$
Preferred orientation correction: none

The crystal structure was refined according to the Rietveld method (Rietveld, 1969) using the *GSAS* program package (Larson & von Dreele, 1984). Initially, only lattice parameters, six peak-shape parameters of the pseudo-Voigt function, one asymmetry parameter and one parameter for the zero-point correction were refined without a structure model according to the LeBail method (LeBail *et al.*, 1988). The high background at low 2θ caused by the position sensitive detector was removed by the fixed background subtraction feature of the *GSAS* program package. Remaining background was fitted with six parameters using a power series function.

No extra reflections were found in the temperature range from 573 to 473 K with respect to hexagonal AlPO₄ tridymite; however, except for 00*l*, all reflections were broadened or split, indicating a monoclinic deformation of the unit cell (see Fig. 2*a*). The extinctions are compatible with space groups $P112_1$ (No. 4) and $P112_1/m$ (No. 11). The latter was rejected since $P112_1/m$ is not a subgroup of $P6_3mc$ (No. 186), which is the symmetry of the hexagonal high-temperature form, and since a mirror plane perpendicular to the pseudo-hexagonal *c* axis is incompatible with an ordered arrangement of the Al and P atoms in the tetrahedral framework. The atomic coordinates of the hexagonal high-temperature phase at 593 K (Graetsch, 2001*a*) were used as starting parameters. The *z* parameter of Al was fixed in order to define the origin.

The wavevector of the modulated phase was refined to $q = 0.0068 (1)a* + 0.006 (1)b*$ at 463 K with the program *JANA*2000 (Petricek & Dusek, 2000). The average structure of the incommensurate phase was refined with *GSAS*, neglecting the weak satellite reflections.

Soft constraints were applied to the interatomic distances, keeping the sizes of the tetrahedra close to those of AlPO₄ quartz [Al—O = 1.73, O—O = 2.83, P—O = 1.52 and O—O = 2.49 Å (Muraoka & Kihara, 1997)], but refined to smaller values. The change from individual isotropic to anisotropic displacement parameters reduced the $R(F^2)$ value from 0.084 to 0.040 for the basic structure at 473 K and from 0.098 to 0.038 for the average structure of the incommensurate phase at 463 K, with an increase from 47 to 77 refined parameters. Corrections for absorption and extinction were found to be unnecessary. Preferred orientation was not observed. The obtained s.u.'s of the atomic coordinates and displacement parameters were multiplied with a factor of three in order to account for possible serial correlations leading to artificially low standard deviations (*cf.* Hill & Flack, 1987; Baerlocher & McCusker, 1994).

For both determinations, data collection: *DIFFRAC-AT* (Version 3.0; Siemens, unpublished); cell refinement: *GSAS* (Larson & von Dreele, 1994); data reduction: *GSAS*; program(s) used to solve structure: *GSAS*; program(s) used to refine structure: *GSAS*; molecular graphics: *ORTEP*-3 (Farrugia, 1997) and *WATOMS* (Dowty, 1994).

References

Baerlocher, C. & McCusker, L. B. (1994). *Advanced Zeolite Science and Applications*, ch. 13, pp. 391–428. Amsterdam: Elsevier Science.
Dowty, E. (1994). *WATOMS*. Shape Software, 521 Hidden Valley Road, Kingsport, Tennessee, USA.
Farrugia, L. J. (1997). *J. Appl. Cryst.* **30**, 565.
Graetsch, H. (2001*a*). *Phys. Chem. Miner.* **28**, 313–321.
Graetsch, H. (2001*b*). *Acta Cryst.* C**57**, 665–667.
Hill, R. J. & Flack, H. D. (1987). *J. Appl. Cryst.* **20**, 356–361.
Kihara, K., Matsumoto, T. & Imamura, M. (1986). *Z. Kristallogr.* **177**, 27–38.
Larson, A. C. & von Dreele, R. B. (1994). *LANSCE*, MS-H805. LANL Report LAUR 86–748. Los Alamos National Laboratory, New Mexico, USA.
LeBail, A., Duroy, H. & Fourquet, J. L. (1988). *Mater. Res. Bull.* **23**, 447–452.
Muraoka, Y. & Kihara, K. (1997). *Phys. Chem. Miner.* **24**, 243–253.
Nukui, A., Yamamoto, A. & Nakazawa, H. (1979). AIP Conference Proc. No. 53, pp. 327–329.
Petricek, V. & Dusek, M. (2000). *JANA*2000. Institute of Physics, Academy of Sciences of the Czech Republic, Praha, Czech Republic.
Pryde, A. K. A. & Dove, M. T. (1998). *Phys. Chem. Miner.* **26**, 171–179.
Rietveld, H. M. (1969). *J. Appl. Cryst.* **2**, 65–71.
Spiegel, M., Hoffmann, W. & Löns, J. (1990). *Eur. J. Mineral.* **2**, 246.